Facile Synthesis of Co_3O_4@CNT with High Catalytic Activity for CO Oxidation under Moisture-Rich Conditions

Chung-Hao Kuo,[†] Weikun Li,[†] Wenqiao Song,[†] Zhu Luo,[†] Altug S. Poyraz,[†] Yang Guo,[‡] Anson W. K. Ma,[‡] Steven L. Suib,*[,†,‡] and Jie He*[,†]

[†]Department of Chemistry and [‡]Institute of Materials Science, University of Connecticut, Storrs, Connecticut 06269, United States

S *Supporting Information*

ABSTRACT: The catalytic oxidation reaction of CO has recently attracted much attention because of its potential applications in the treatment of air pollutants. The development of inexpensive transition metal oxide catalysts that exhibit high catalytic activities for CO oxidation is in high demand. However, these metal oxide catalysts are susceptible to moisture, as they can be quickly deactivated in the presence of trace amounts of moisture. This article reports a facile synthesis of highly active Co_3O_4@CNT catalysts for CO oxidation under moisture-rich conditions. Our synthetic routes are based on the in situ growth of ultrafine Co_3O_4 nanoparticles (NPs) (~2.5 nm) on pristine multiwalled CNTs in the presence of polymer surfactant. Using a 1% CO and 2% O_2 balanced in N_2 (normal) feed gas (3−10 ppm moisture), a 100% CO conversion with Co_3O_4@ CNT catalysts was achieved at various temperatures ranging from 25 to 200 °C at a low O_2 concentration. The modulation of surface hydrophobicity of CNT substrates, other than direct surface modification on the Co_3O_4 catalytic centers, is an efficient method to enhance the moisture resistance of metal oxide catalysts for CO oxidation. After introducing fluorinated alkyl chains on CNT surfaces, the superhydrophobic Co_3O_4@CNT exhibited outstanding activity and durability at 150 °C in the presence of moisture-saturated feed gas. These materials may ultimately present new opportunities to improve the moisture resistance of metal oxide catalysts for CO oxidation.

KEYWORDS: CO oxidation, Co_3O_4 nanoparticles, carbon nanotube, superhydrophobicity, hydrophobic catalysts, metal oxide catalysts
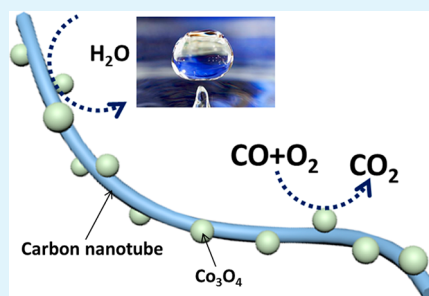
INTRODUCTION

Carbon monoxide (CO) from the incomplete combustion of hydrocarbon fuels is one of the major air pollutants.[1] The catalytic oxidation reaction of CO has become increasingly important for diminishing the emission of CO through the pretreatment of effluent gas from various industrial sources and automobile exhaust. Although noble metal catalysts or supported noble metal catalysts (i.e., Pt, Pd, and Au) have proven to be the most active,[2−8] the high cost of such catalysts largely limits their extensive application. In this context, inexpensive metal oxide catalysts have recently attracted attention. Particularly, Co_3O_4, CuO, and MnO_2 exhibit high catalytic activities for CO oxidation.[9−19] Metal oxide catalysts, like Co_3O_4, however, are susceptible to moisture, as they can be quickly deactivated in the presence of trace amounts of moisture (>3 ppm). To date, the development of highly active Co_3O_4 catalysts for CO oxidation that operate under high moisture conditions is still very challenging. Recent reports have demonstrated that nanostructures[13−17,20] and surface properties of Co_3O_4 catalysts[10,18,19,21] play important roles in the activity of catalysts under high moisture conditions. On one hand, the active species of Co^{3+} cations are distributed on (110) facets of the spinel structure Co_3O_4.[22] The synthesized nanostructures that can selectively expose such facets are particularly beneficial for their catalytic activity. Xie et al. reported that Co_3O_4 nanorods were much less sensitive to

water and were highly active for CO oxidation at low temperature (−77 °C) using normal feed gas (3−10 ppm moisture).[14] The predominant exposure of (110) facets, which enriched active species of Co^{3+} on the surfaces along the nanorods, resulted in efficient interactions with CO. On the other hand, the hydrophobicity of the catalyst surface disrupts the affinity of water toward the Co_3O_4 surface. For example, Co_3O_4 coated with hydrophobic poly(dimethylsiloxane) can prevent deactivation of catalysts in the presence of water.[10] However, the active sites/surface of these catalysts can be easily blocked by hydrophobic coatings, thus decreasing catalytic efficiency.

In the present study, we report a facile and robust wet-chemical approach to synthesize Co_3O_4@CNT with high catalytic activity for CO oxidation. Carbon nanotubes (CNTs) with large surface area have been widely used as 1D substrates to support the growth of various nanostructured Co_3O_4.[23−32] The synthetic route herein is based on the in situ growth of ultrafine Co_3O_4 nanoparticles (NPs) on pristine multiwalled CNTs (Figure 1), without any covalent functionalization or chemical oxidation of the CNT surface. By controlling the hydrophobicity of CNT substrates, other than by the direct

surface modification of Co_3O_4 catalytic centers, Co_3O_4@CNT catalysts are markedly active for CO oxidation, and 100% CO conversion is achieved using moisture-saturated (~3%) feed gas. Our approach thus stands out as a promising pathway to synthesize highly efficient catalysts on CNTs. These materials may ultimately present new opportunities to improve the moisture resistance of metal oxide catalysts for CO oxidation.

■ EXPERIMENTAL SECTION

Materials. All chemical reagents were purchased from Aldrich and used without further purification unless otherwise noted. 2-(2-Methoxyethoxy)ethyl methacrylate (MEO$_2$MA, 95%), *tert*-butyl acrylate (98%), and styrene (99.9%) were passed through a basic aluminum oxide column prior to use. Azobis(isobutyronitrile) (AIBN) was recrystallized from ethanol. Pristine multiwalled CNTs (Southwest Nanotechnologies Inc.) with diameters of ~10 nm and an aspect ratio >350−550 were used as received. Commercial Co_3O_4 (99.5%) was obtained from Strem Chemical Inc. and used as received.

Synthesis of Co_3O_4 NPs. Co_3O_4 NPs were synthesized using a reported procedure with a slight modification.[38] Briefly, 500 mg of cobalt(II) acetate tetrahydrate (Co(II)Ac$_2$) as a precursor for Co_3O_4 NP growth was first dissolved in 30 mL of water/ethanol solution (1:1, v/v) at 45 °C. Three milliliters of ammonium hydroxide (27−30 vol %) solution was added dropwise to the above solution under strong stirring. The reaction mixture was then heated to reflux for 3 h. After cooling to room temperature, the reaction suspension was centrifuged at 4500 rpm for 20 min in the presence of 100 mL of acetone. The collected precipitates were redispersed in 100 mL of ethanol and washed twice with acetone by centrifugation. The final product of Co_3O_4 NPs was dried under vacuum at 60 °C.

Synthesis and the Fluorination of Co_3O_4@CNT. The synthesis details of polymer surfactant composed of poly(2-(2-methoxyethoxy)-ethyl methacrylate (PMEO$_2$MA) and poly(styrene-*co*-acrylic acid) (PMEO$_2$MA$_{84}$-*b*-P(St$_{61}$-*co*-tAA$_5$)) are given in the Supporting Information. The polymer surfactant of PMEO$_2$MA$_{84}$-*b*-P(St$_{61}$-*co*-tAA$_5$) has a M_n(GPC) of 38.5 kg/mol and a polydispersity index (M_w/M_n) PDI = 1.22. For the synthesis of Co_3O_4@CNT, 5 mg of PMEO$_2$MA$_{84}$-*b*-P(St$_{61}$-*co*-tAA$_5$) was first mixed with 5 mg of CNTs in 15 mL of dimethylformamide. The uniform suspension was obtained after sonication for 2 min at room temperature. About 3 mL of the suspension (~1 mg of CNTs) was then mixed with 3 mL of Co(II)Ac$_2$ ethanol solution (30 mg of Co(II)Ac$_2$ in 3 mL of ethanol). After sonication for another 2 min, 0.1 mL of ammonia hydroxide (27−30 vol %) was quickly injected into the above solution under magnetic stirring. The reaction was then heated at 85 °C and refluxed for 3 h. After cooling, the reaction suspension was centrifuged at 6000 rpm for 15 min. The collected precipitates were washed with ethanol and centrifuged another three times to remove the unreacted precursors and unattached Co_3O_4 NPs. The final product was dried under vacuum at 40 °C. The fluorination of Co_3O_4@CNT was performed by using the vapor phase deposition technique. Co_3O_4@CNT (100 mg) was loaded into a 100 mL sealed jar and pretreated at 80 °C for 30 min. Subsequently, 50 μL of 1*H*,1*H*,2*H*,2*H*-perfluorodecyltriethoxysilane (PFDTES) was added to a 4 mL vial and quickly loaded into a sealed jar. After 1 h, 50 μL of PFDTES was added again using the above method. After silanation for another 1 h, the fluorinated Co_3O_4@CNT (F−Co_3O_4@CNT) was obtained.

CO Oxidation of Co_3O_4@CNT and F−Co_3O_4@CNT. The CO oxidation reaction was carried out in a continuous flow fixed-bed glass tubular reactor under atmospheric pressure. As-prepared catalyst (100 mg) was used for each test. Before the measurement, the catalyst was pretreated at 200 °C for 1 h under air and another 1 h under helium flow to clean the catalyst surface. After loading the catalysts in the glass tubular reactor, a gas mixture containing 1% CO and 2% O$_2$ balanced in N$_2$ (normal feed gas) was passed through the catalyst bed. The outlet gas streams were analyzed with an online gas chromatograph (SRI 8610C multiple gas analyzer #1 GC) equipped with a thermal conductivity detector (TCD), a 6 foot long molecular sieve 13X packed column, and a 6 foot long silica gel packed column. The

reaction temperature was measured using a K-type thermocouple inserted directly into the catalyst bed. GC samples were injected after 10 min stabilization at any given temperature. The reaction conversion was calculated on the basis of CO concentration, using nitrogen as an internal standard. Normal gas conditions were obtained by using the as-mixed normal feed gas (~3 ppm of water vapor). Wet conditions were obtained by passing the feed gas through a water bubbler at room temperature (~3% of water vapor). To protect the GC column, moisture was trapped by desiccant before the outlet gas streams entered the GC.

Other Characterizations. Size-exclusion chromatography (SEC) measurements were performed on a Malvern system equipped with a Viscotek RI detector and D6000M column (300 × 8.0 mm). Dimethylformamide was used as the carrier solvent at a flow rate of 0.7 mL/min, and polystyrene standards (Polymer Laboratories, Inc.) were used for calibration. The data were processed using OmniSEC software. ^{1}H NMR spectra were recorded on a Bruker Avance 300 MHz spectrometer. The crystallinity of Co_3O_4@CNT materials was characterized using a Rigaku UltimaIV powder X-ray diffractometer with Cu Kα radiation, a beam voltage of 40 kV, and beam current of 44 mA. High-resolution transmission electron microscopy (HRTEM) studies were carried out using a JEOL 2010 transmission electron microscope with an accelerating voltage of 200 kV. The TEM samples were prepared by casting the suspension of Co_3O_4@CNT (3−5 μL in ethanol) on a carbon-coated copper grid (300 mesh). Thermogravimetric analyses (TGA) were performed on a Hi-Res TA 2950 thermogravimetric analyzer with 60 mL/min of air flow from 25 to 1000 °C at a heating rate of 10 °C/min. The evaluation of cobalt content on the surface of CNTs was carried out on a Varian AA-4 updated atomic absorption spectrometer (AAS) with a hollow cathode lamp and a deuterium background corrector at the respective resonance line using an air−acetylene flame. The as-synthesized samples were digested with aqua regia, and then insoluble CNTs were filtered out. The collected filtrates were diluted with deionized water and used for analyzing the concentration of cobalt ions. The X-ray photoelectron spectra (XPS) surface analyses were performed on a PHI model 590 spectrometer with multiprobes (Physical Electronics Industries Inc.) using Al Kα radiation (λ = 1486.6 eV) as the radiation source. The powder samples were pressed on carbon tape mounted on adhesive copper tape stuck to a sample stage placed in the analysis chamber. The water contact angles (CA) were measured on a Dataphysics OCA20 contact-angle system at ambient temperature. The sample was uniformly mounted on double-sided carbon tape, with one side stuck on a glass slide. Three microliters of distilled water was slowly dropped onto the surface of the carbon tape coated with various samples. Reported CA values are averages of three independent measurements. Attenuated total reflection Fourier transform infrared (ATR-FTIR) spectra were recorded using a ThermoScientific Nicolet iS5 spectrometer by directly placing samples on a germanium crystal. The Brunauer−Emmett−Teller (BET) surface area of catalysts was measured using a Quantachrome Autosorb-1-C automated N$_2$ gas adsorption system. Fifty milligrams of samples was degassed at 150 °C for 12 h to remove water and other physically adsorbed species.

■ RESULTS AND DISCUSSION

The in situ growth of Co_3O_4 NPs on CNTs was assisted by a polymer surfactant of poly(2-(2-methoxyethoxy)ethyl methacrylate (PMEO$_2$MA) and poly(styrene-*co*-acrylic acid) (PMEO$_2$MA-*b*-P(St-*co*-AA), with 8 mol % of AA units in styrene block) (see Supporting Information for polymer synthesis and characterizations). The polymer surfactant is composed of an inert block of PMEO$_2$MA and a functional block of P(St-*co*-AA), where styrene units can interact with CNTs through $\pi−\pi$ interactions and carboxylic acid moieties can coordinate with Co ions via electrostatic forces.[33−36] The inert PMEO$_2$MA block is essential to enable the good solubility of polymer surfactants under high ionic strength. For example, the polymer surfactant of PMEO$_2$MA-*b*-P(St-*co*-AA) can
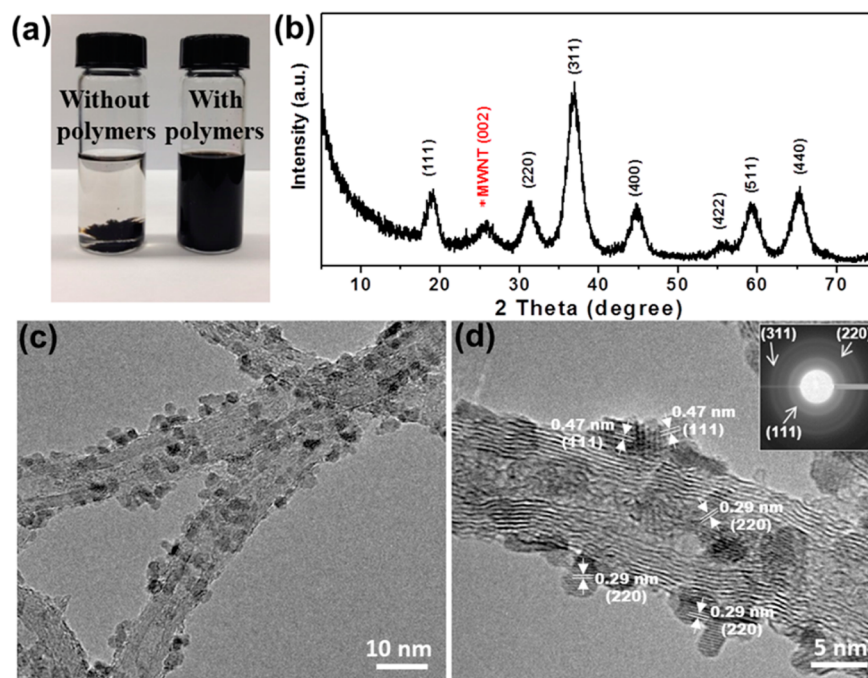
Figure 1. (a) Images of pristine CNTs (left) and CNTs with polymer surfactants (right) in dimethylformamide taken after sonication and overnight incubation. The CNTs can form a stable suspension in the presence of polymer surfactants. (b) Powder XRD pattern for synthesized Co_3O_4@CNT catalysts. The peak located at 26° is ascribed to CN (002) reflections. (c, d) High-magnification TEM images of Co_3O_4@CNT catalysts. The measured size of Co_3O_4 NPs is 2.5 ± 0.5 nm by averaging more than 100 NPs. The inset in panel d is the selected-area electron diffraction pattern of Co_3O_4@CNT.

stabilize the suspension of CNTs even at ∼30 mM of cobalt salts. In a typical synthesis, $PMEO_2MA$-b-P(St-co-AA) and CNTs (∼10 nm in diameter) (1:1, wt %) were first mixed in dimethylformamide. As a result of strong π−π interactions of CNTs with aromatic rings on P(St-co-AA) blocks (see Figure S2), a uniform suspension could be obtained after sonication for 2 min at room temperature (Figure 1a).[33−36] Given the small fraction of carboxylic acid groups in P(St-co-AA) blocks coordinating with Co ions, the Co_3O_4 NPs can thus easily nucleate and grow on the surface of CNTs following the addition of cobalt(II) acetate and ammonium hydroxide in the mixed solvent of ethanol, dimethylformamide, and water at 80 °C.[37,38] Ammonia hydroxide can steadily mediate the hydrolysis and oxidation of Co ions, and the loading amount of Co_3O_4 NPs on CNTs can be readily controlled by the amount of cobalt(II) acetate (see Figure S4). Compared to the covalent functionalization treatment of CNTs where the aggressive chemical oxidations can alter the orbital hybridization of carbon atoms from sp^2 to sp^3 and disrupt the band-to-band transitions of π electrons of CNTs,[39−41] the non-covalent functionalization of CNTs is based on the weak π−π interactions with polymer surfactants and has the advantages of (i) simple and mild reaction conditions, (ii) no strong redox reactions involved on tubular body (see Raman discussion below), and (iii) facile yet general approach that can be applied to the in situ growth of other metal oxide NPs, e.g., TiO_2, Mn_3O_4, and CeO_2 (see Figure S5). This may illustrate an alternative and simple approach for the in situ growth of NPs on CNT surfaces via the noncovalent bonding of polymer surfactants.

Figure 1c,d presents representative transmission electron microscopy (TEM) images of Co_3O_4@CNT at high magnifications (see Figure S3 for lower-magnification TEM images).

Spherical Co_3O_4 NPs are uniformly decorated on CNT surfaces, and they are fairly monodispersed, with an average diameter of 2.5 ± 0.5 nm. The high-resolution TEM image of Co_3O_4 NPs clearly shows the crystalline nature of individual Co_3O_4 NPs (Figure 1d). The interplanar distances with the d-spacings of 0.47 and 0.29 nm correspond to the (111) and (220) facets of spinel Co_3O_4, respectively. The powder X-ray diffraction patterns in Figure 1b show strong diffraction peaks of the (111), (220), and (311) facets, indexed to the cubic spinel structure of Co_3O_4 NPs (JCPDS card no: 00-043-1003), in accordance with the TEM observation. The loading amount of Co_3O_4 NPs on CNTs estimated from atomic absorption measurements (digesting Co_3O_4 NPs from CNTs using aqua regia solution) is approximately 43 wt %, calculated from the Co standard calibration curve. The estimated amount of Co_3O_4 on CNTs collected from atomic absorption measurements is slightly larger than thermogravimetric measurements (see Figure S7). Due to supporting the catalyst on CNTs with a very large surface-to-volume ratio, the Co_3O_4@CNT catalyst has a BET surface area of 143 m^2/g and pore volume of 0.67 cm^3/g, notably higher than nanosized Co_3O_4 NPs and commercial Co_3O_4 materials (Table S2).

The noncovalent bonding of CNTs and polymers does not alter their electronic structures, as evidenced by Raman spectra (Figure 2a). The D- and G-bands of multiwalled CNTs for pristine CNTs, polymer/CNTs, and Co_3O_4@CNT appear at 1354 and 1598 cm^{-1}, respectively, assigned to the defects and disorder-induced mode and in-planar E_{2g} zone-center mode.[42,43] No obvious shift of the D- and G-bands of CNTs was observed after polymer modification and the growth of Co_3O_4 NPs. In addition, the intensity ratios of the D- and G-bands (I_D/I_G) for pristine CNTs, polymer/CNTs, and Co_3O_4@CNT are 1.09, 1.11, and 1.06, respectively. This suggests that
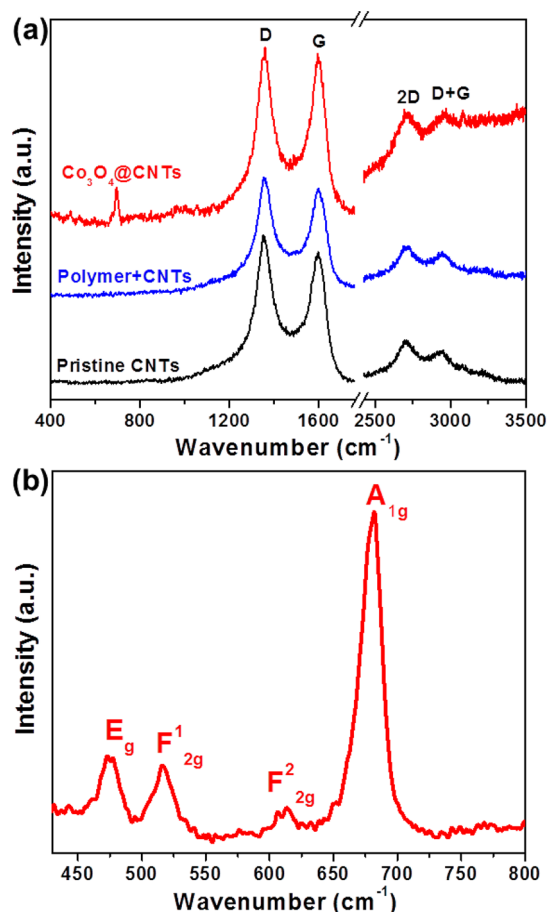
Figure 2. (a) Raman spectra of pristine CNTs, CNTs with polymers, and Co_3O_4@CNT. The D, G, 2D, and D + G bands are defect-related peaks of CNT or amorphous carbon. No shift of these peaks was observed after mixing with polymers and the growth of Co_3O_4, indicating that the surface of CNTs was not chemically modified. (b) Close observation of Raman-active lattice vibrations of Co_3O_4.

such noncovalent functionalization of CNTs preserves their pristine surface and does not introduce further defects on the tubular body. The formation of Co_3O_4 NPs was further confirmed by Raman spectra as well (Figure 2b). Four Raman-active lattice vibrations appear at 477, 516, 612, and 682 cm^{-1}, indicating the cubic spinel structure of Co_3O_4 NPs.

To investigate the catalytic activity, the obtained Co_3O_4@CNT was first pretreated by annealing at 200 °C under atmosphere for 1 h. After loading ∼100 mg of activated catalyst (∼43 mg of Co_3O_4) into a glass tubular reactor, the CO oxidation reaction was carried out under a continuous flow of a normal gas mixture containing 1% CO and 2% CO_2 balanced in 97% of N_2 (space velocity of 35 000 mL g^{-1} h^{-1} and moisture of 3−10 ppm). The catalytic performance of Co_3O_4@CNT is given in Figure 3. A 100% conversion of CO to CO_2 was achieved at various temperatures ranging from 25 to 200 °C at a low O_2 concentration. The high catalytic activity is likely attributed to nanosized Co_3O_4 particles supported on CNTs having a much larger specific surface area of 143 m^2/g and pore volume of 0.67 cm^3/g.[38,44−46] These results suggest that more active sites on Co_3O_4@CNT catalysts can be exposed. The free Co_3O_4 NPs synthesized without CNT supports and commercial Co_3O_4 catalysts show only little activity for CO oxidation at room temperature (see Figures S9 and S10). The T_{50} (50% CO conversion at this temperature) of free Co_3O_4 NPs and
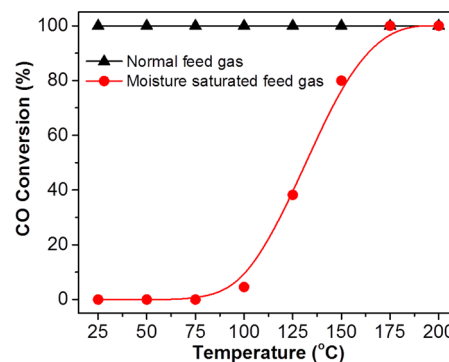
Figure 3. Temperature dependence of catalytic activity of Co_3O_4@CNT catalysts for CO oxidation. The CO conversion was measured and quantified by gas chromatography. Each data point was collected after stabilizing the catalysts under feed gas conditions and temperature for at least 10 min.

commercial Co_3O_4 catalysts is ∼86 and ∼178 °C, respectively. Subsequently, the Co_3O_4@CNT catalysts have been tested using moisture-saturated feed gas (∼3% water) close to the water concentration of automobile exhaust (Figure 3).[47] Under such a critical environment, the light-off temperature of Co_3O_4@CNT catalysts is ∼100 °C, and the T_{50} is ∼132 °C. The catalytic activity at higher temperatures ($T > 175$ °C) is not affected. When the temperature is further decreased, the CO conversion drops rapidly. For example, only 80% of CO was converted into CO_2 at $T = 150$ °C. The commercial Co_3O_4 catalysts are completely inactive under such conditions at $T = 200$ °C (see Figure S9).

The surface hydrophobicity of Co_3O_4@CNT catalysts is assumed to influence the moisture resistance of catalysts. In order to optimize moisture resistance, we have further modified the Co_3O_4@CNT surface using the fluorination of PFDTES. The residual −COOH groups from the polymers can selectively react with PFDTES to introduce fluorinated alkyl chains that alter the hydrophobicity of catalysts. Through the vapor phase deposition technique, the Co_3O_4@CNT catalysts were treated with PFDTES vapor at 80 °C for 30 min. The fluorinated coating on the surface of Co_3O_4@CNT is further confirmed by X-ray photoelectron spectra (XPS) (Figures 4 and S8). The F 1s peak at 688 eV is assigned to fluorinated alkyl chains of PFDTES.[48] The Co $2p_{1/2}$ and $2p_{3/2}$ areas did not
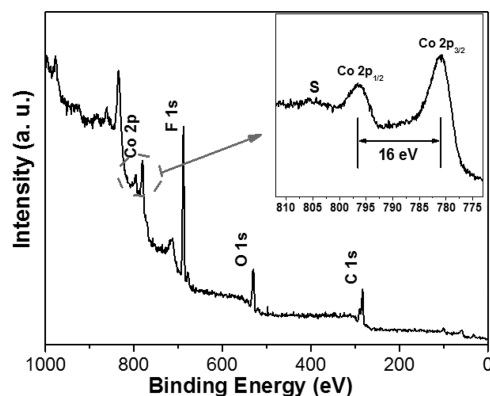
Figure 4. X-ray photoelectron spectrum of F−Co_3O_4@CNT catalysts. The appearance of F 1s signals at 688 eV is assigned to the PFDTES coating. The inset is the Co 2p signals, correlated to Co $2p_{3/2}$ (780.8 eV) and Co $2p_{1/2}$ (796.5 eV) peaks.

show any significant differences following the fluorination treatment, indicating that the terminal silane groups of PFDTES are bonded to CNT substrates other than Co_3O_4 NPs.[49] The fact that the active sites on Co_3O_4 were preserved is particularly important.

Figure 5 presents the CO conversion curves of $F-Co_3O_4@$ CNT at various temperatures. Again, when using normal feed
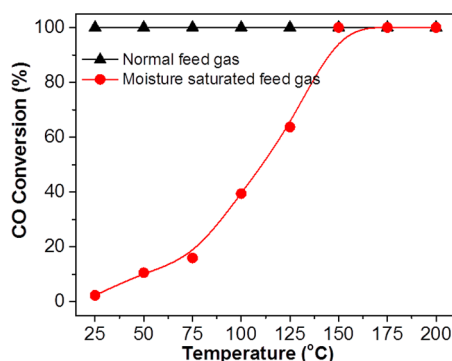
Figure 5. Temperature dependence of catalytic activity of $F-Co_3O_4@$ CNT catalysts for CO oxidation. The CO conversion was measured and quantified by gas chromatography. Each data point was collected after stabilizing the catalysts under feed gas conditions and temperature for at least 10 min.

gas, 100% CO conversion was obtained at various temperatures. This confirms that the fluorination of $Co_3O_4@CNT$ did not shield the surface of Co_3O_4 and therefore did not prevent adsorption of CO and O_2 on the catalytic center. Under saturated moisture, the shift of the CO conversion curve to lower temperature is obvious compared to that of bare $Co_3O_4@CNT$ catalysts. The light-off temperature of $F-Co_3O_4@CNT$ catalysts is ~40 °C, and T_{50} is ~110 °C, corresponding to a 22 °C decrease compared to that of nonfluorinated $Co_3O_4@CNT$. At $T = 150$ °C, the CO conversion can still reach 100% for $F-Co_3O_4@CNT$. This is the lowest light-off and T_{100} temperature of Co_3O_4 NPs under saturated moisture so far. The improved moisture resistance of $F-Co_3O_4@CNT$ is attributed to the increase in the surface hydrophobicity of the catalysts, which prevents water accumulation on the surface of Co_3O_4 active sites.

The changes of surface hydrophobicity of catalysts were confirmed by water contact angle measurements. The powder samples of catalysts were pressed onto carbon tape mounted on adhesive copper tape stuck to form a condensed film. From water contact angles (Figure 6a–c), our $Co_3O_4@CNT$ catalysts, having a contact angle of 108.8°, are more hydrophobic than pure Co_3O_4 particles, which have a contact angle of 86.1°. The surface hydrophobicity of CNTs slightly improved the moisture resistance of catalysts, as evidenced by 100% CO conversion achieved in the presence of 3−10 ppm moisture. However, the hydrophobicity is not high enough to repel the moisture at higher water content (3% of moisture). After surface treatment by PFDTES, the contact angle of fluorinated $Co_3O_4@CNT$ ($F-Co_3O_4@CNT$) further increased to 142.4° (Figure 6c), indicating the superhydrophobicity of $F-Co_3O_4@CNT$. The fluorinated alkyl chains of PFDTES can form a hydrophobic layer on CNTs that enhances the hydrophobicity of $F-Co_3O_4@CNT$. The hydrophobic layer does not block the active sites on Co_3O_4, as evidenced by the catalytic activity of $F-Co_3O_4@CNT$ with normal feed gas.
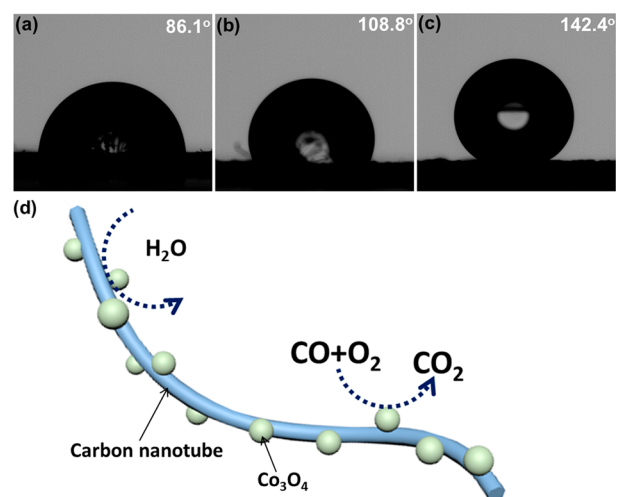
Figure 6. (a−c) Contact angle measurements of commercial Co_3O_4 (a), $Co_3O_4@CNT$ (b), and $F-Co_3O_4@CNT$ (c) catalysts. (d) Schematic illustration of surface hydrophobicity of catalysts, which prevents water accumulation on the surface of the catalysts.

Thus, the improved hydrophobicity of the CNT substrate only shields the moisture from the active sites, resulting in the decrease of light-off and T_{50} temperature for $F-Co_3O_4@CNT$ (Figure 6d).

To gain further insight on the effect of surface properties, we examined the kinetics of moisture deactivation of two catalysts. Figure 7 presents a time-resolved study of the catalytic
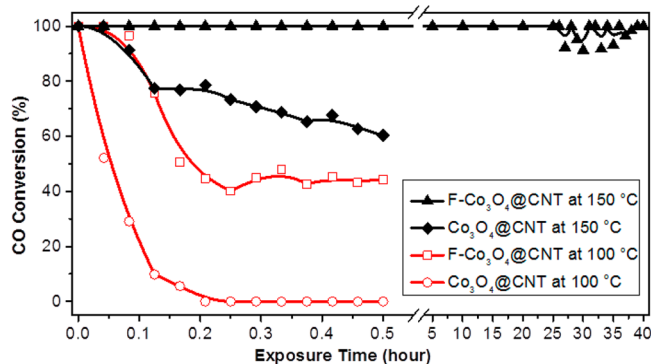
Figure 7. Time-resolved study of the catalytic performance of $Co_3O_4@CNT$ and $F-Co_3O_4@CNT$ at 150 and 100 °C using moisture-saturated feed gas. For the long-term stability test, the moisture-saturated gas was continuously passed through the catalysts, and the moisture was removed before the CO conversion measurement.

performance of $Co_3O_4@CNT$ and $F-Co_3O_4@CNT$ at 150 and 100 °C as a function of water exposure time. At $T = 150$ °C, $F-Co_3O_4@CNT$ showed high catalytic performance and 100% CO conversion was reached regardless of the water exposure time. The bare $Co_3O_4@CNT$ showed a continuous decrease of CO conversion when the water exposure time was increased to 30 min. This suggests that water can still accumulate around the catalytic centers and gradually deactivate the catalysts. At this point, the turnover frequency of $F-Co_3O_4@CNT$ is 3.31×10^{-4} s^{-1}, which is nearly twice as high as 1.86×10^{-4} s^{-1} of $Co_3O_4@CNT$ (based on the total mass of Co ions). When the temperature dropped to 100 °C, the CO conversion of $F-CO_3O_4@CNT$ decreased in the first

10 min and remained at ∼50%. Co$_3$O$_4$@CNT, on the other hand, quickly deactivated within 10 min. This observation implies that the water adsorption rate on the CO$_3$O$_4$@CNT catalyst surface is higher than the water desorption rate at 100 °C; the accumulation of water would gradually passivate the catalytic sites. On the contrary, the adsorption rate on the F−CO$_3$O$_4$@CNT is much lower due to the surface hydrophobicity, and water does not accumulate.

Finally, the long-term stability of F−CO$_3$O$_4$@CNT catalysts was studied at 150 °C under moisture-saturated conditions (Figure 7). The catalytic activity of F−CO$_3$O$_4$@CNT is extremely stable. This catalyst gave 100% conversion of CO after 26 h, and a small fluctuation of CO conversion appeared after that. The loss of stability is probably due to partial detaching/degradation of fluorinated PFDTES on the catalyst surface as well as an accumulation of carbonate species on the surface. The nanostructure of the catalysts did not change after the catalytic tests at 150 °C for 40 h (data not shown). Overall, the F−CO$_3$O$_4$@CNT catalysts have shown high durability for CO conversion under a harsh environment.

■ CONCLUSIONS

In summary, we have developed a polymer-assisted, facile synthesis of highly active Co$_3$O$_4$@CNT catalysts for CO oxidation under moisture-rich conditions. The modulation of surface hydrophobicity of CNT substrates was demonstrated to be an efficient method to enhance the moisture resistance of metal oxide catalysts for CO oxidation. Using moisture-saturated feed gas, the fluorinated Co$_3$O$_4$@CNT exhibited an outstanding activity and durability at 150 °C. This approach is simple and fast, yet general, and can be potentially applied to other types of metal oxide catalysts. This research may open up a new realm of possibilities in developing inexpensive and moisture-resistant metal oxide catalysts for CO oxidation.

■ ASSOCIATED CONTENT

Ⓢ Supporting Information

Synthesis details and additional characterization of polymers and catalysts. This material is available free of charge via the Internet at http://pubs.acs.org.

■ AUTHOR INFORMATION

Corresponding Authors
*(S.L.S.) E-mail: steven.suib@uconn.edu.
*(J.H.) E-mail: jie.he@uconn.edu.
Notes
The authors declare no competing financial interest.

■ ACKNOWLEDGMENTS

■ REFERENCES

(1) Pommier, M.; McLinden, C. A.; Deeter, M. Relative Changes in CO Emissions over Megacities Based on Observations from Space. *Geophys. Res. Lett.* **2013**, *40*, 3766−3771.

(2) Min, B. K.; Friend, C. M. Heterogeneous Gold-Based Catalysis for Green Chemistry: Low-Temperature CO Oxidation and Propene Oxidation. *Chem. Rev.* **2007**, *107*, 2709−2724.

(3) Imanaka, N.; Masui, T.; Imadzu, H.; Yasuda, K. Carbon Monoxide Oxidation at Room Temperature on Pt/CeO$_2$−ZrO$_2$−Bi$_2$O$_3$ Catalysts. *Chem. Commun.* **2011**, *47*, 11032−11034.

(4) Carrettin, S.; Concepción, P.; Corma, A.; López Nieto, J. M.; Puntes, V. F. Nanocrystalline CeO$_2$ Increases the Activity of Au for CO Oxidation by Two Orders of Magnitude. *Angew. Chem., Int. Ed.* **2004**, *43*, 2538−2540.

(5) Comotti, M.; Li, W.-C.; Spliethoff, B.; Schüth, F. Support Effect in High Activity Gold Catalysts for CO Oxidation. *J. Am. Chem. Soc.* **2006**, *128*, 917−924.

(6) Liu, L. M.; McAllister, B.; Ye, H. Q.; Hu, P. Identifying an O$_2$ Supply Pathway in CO Oxidation on Au/TiO$_2$(110): A Density Functional Theory Study on the Intrinsic Role of Water. *J. Am. Chem. Soc.* **2006**, *128*, 4017−4022.

(7) Gong, J.; Mullins, C. B. Selective Oxidation of Ethanol to Acetaldehyde on Gold. *J. Am. Chem. Soc.* **2008**, *130*, 16458−16459.

(8) Herzing, A. A.; Kiely, C. J.; Carley, A. F.; Landon, P.; Hutchings, G. J. Identification of Active Gold Nanoclusters on Iron Oxide Supports for CO Oxidation. *Science* **2008**, *321*, 1331−1335.

(9) Royer, S.; Duprez, D. Catalytic Oxidation of Carbon Monoxide over Transition Metal Oxides. *ChemCatChem.* **2011**, *3*, 24−65.

(10) Chen, C.-H.; Njagi, E. C.; Sun, S.-P.; Genuino, H.; Hu, B.; Suib, S. L. Hydrophobic Polymer-Coated Metal Oxide Catalysts for Effective Low-Temperature Oxidation of CO under Moisture-Rich Conditions. *Chem. Mater.* **2010**, *22*, 3313−3315.

(11) Jansson, J.; Palmqvist, A. E. C.; Fridell, E.; Skoglundh, M.; Österlund, L.; Thormählen, P.; Langer, V. On the Catalytic Activity of Co$_3$O$_4$ in Low-Temperature CO Oxidation. *J. Catal.* **2002**, *211*, 387−397.

(12) Dangwal Pandey, A.; Jia, C.; Schmidt, W.; Leoni, M.; Schwickardi, M.; Schüth, F.; Weidenthaler, C. Size-Controlled Synthesis and Microstructure Investigation of Co$_3$O$_4$ Nanoparticles for Low-Temperature CO Oxidation. *J. Phys. Chem. C* **2012**, *116*, 19405−19412.

(13) Jiang, D.-e.; Dai, S. The Role of Low-Coordinate Oxygen on Co$_3$O$_4$(110) in Catalytic CO Oxidation. *Phys. Chem. Chem. Phys.* **2011**, *13*, 978−984.

(14) Xie, X.; Li, Y.; Liu, Z.-Q.; Haruta, M.; Shen, W. Low-Temperature Oxidation of CO Catalysed by Co$_3$O$_4$ Nanorods. *Nature* **2009**, *458*, 746−749.

(15) Sun, Y.; Lv, P.; Yang, J.-Y.; He, L.; Nie, J.-C.; Liu, X.; Li, Y. Ultrathin Co$_3$O$_4$ Nanowires with High Catalytic Oxidation of CO. *Chem. Commun.* **2011**, *47*, 11279−11281.

(16) Teng, Y.; Kusano, Y.; Azuma, M.; Haruta, M.; Shimakawa, Y. Morphology Effects of Co$_3$O$_4$ Nanocrystals Catalyzing CO Oxidation in a Dry Reactant Gas Stream. *Catal. Sci. Technol.* **2011**, *1*, 920−922.

(17) Wang, Y.-Z.; Zhao, Y.-X.; Gao, C.-G.; Liu, D.-S. Preparation and Catalytic Performance of Co$_3$O$_4$ Catalysts for Low-Temperature CO Oxidation. *Catal. Lett.* **2007**, *116*, 136−142.

(18) Yan, N.; Chen, Q.; Wang, F.; Wang, Y.; Zhong, H.; Hu, L. High Catalytic Activity for CO Oxidation of Co$_3$O$_4$ Nanoparticles in SiO$_2$ Nanocapsules. *J. Mater. Chem. A* **2013**, *1*, 637−643.

(19) Yu, Y.; Takei, T.; Ohashi, H.; He, H.; Zhang, X.; Haruta, M. Pretreatments of Co$_3$O$_4$ at Moderate Temperature for CO Oxidation at −80 °C. *J. Catal.* **2009**, *267*, 121−128.

(20) Poyraz, A. S.; Kuo, C.-H.; Biswas, S.; King'ondu, C. K.; Suib, S. L. A General Approach to Crystalline and Monomodal Pore Size Mesoporous Materials. *Nat. Commun.* **2013**, *4*, 29521−295210.

(21) Lin, H. K.; Chiu, H. C.; Tsai, H. C.; Chien, S. H.; Wang, C. B. Synthesis, Characterization and Catalytic Oxidation of Carbon Monoxide over Cobalt Oxide. *Catal. Lett.* **2003**, *88*, 169−174.

(22) Sun, H.; Ang, H. M.; Tade, M. O.; Wang, S. Co$_3$O$_4$ Nanocrystals with Predominantly Exposed Facets: Synthesis, Environmental and Energy Applications. *J. Mater. Chem. A* **2013**, *1*, 14427−14442.

(23) Liang, Y.; Wang, H.; Diao, P.; Chang, W.; Hong, G.; Li, Y.; Gong, M.; Xie, L.; Zhou, J.; Wang, J.; Regier, T. Z.; Wei, F.; Dai, H.

Oxygen Reduction Electrocatalyst Based on Strongly Coupled Cobalt Oxide Nanocrystals and Carbon Nanotubes. *J. Am. Chem. Soc.* **2012**, *134*, 15849−15857.

(24) Wu, J.; Xue, Y.; Yan, X.; Yan, W.; Cheng, Q.; Xie, Y. Co_3O_4 Nanocrystals on Single-Walled Carbon Nanotubes as a Highly Efficient Oxygen-Evolving Catalyst. *Nano Res.* **2012**, *5*, 521−530.

(25) Zhuo, L.; Wu, Y.; Ming, J.; Wang, L.; Yu, Y.; Zhang, X.; Zhao, F. Facile Synthesis of A Co_3O_4−Carbon Nanotube Composite and Its Superior Performance as an Anode Material for Li-Ion Batteries. *J. Mater. Chem. A* **2013**, *1*, 1141−1147.

(26) He, X.; Wu, Y.; Zhao, F.; Wang, J.; Jiang, K.; Fan, S. Enhanced Rate Capabilities of Co_3O_4/Carbon Nanotube Anodes for Lithium Ion Battery Applications. *J. Mater. Chem. A* **2013**, *1*, 11121−11125.

(27) Lu, X.; Zhao, C. Highly Efficient and Robust Oxygen Evolution Catalysts Achieved by Anchoring Nanocrystalline Cobalt Oxides onto Mildly Oxidized Multiwalled Carbon Nanotubes. *J. Mater. Chem. A* **2013**, *1*, 12053−12059.

(28) Xu, M.; Wang, F.; Zhang, Y.; Yang, S.; Zhao, M.; Song, X. Co_3O_4−Carbon Nanotube Heterostructures with Bead-on-String Architecture for Enhanced Lithium Storage Performance. *Nanoscale* **2013**, *5*, 8067−8072.

(29) Yoon, T. H.; Park, Y. J. Polydopamine-Assisted Carbon Nanotubes/Co_3O_4 Composites for Rechargeable Li-Air Batteries. *J. Power Sources* **2013**, *244*, 344−353.

(30) Du, N.; Zhang, H.; Chen, B.; Wu, J. B.; Ma, X. Y.; Liu, Z. H.; Zhang, Y. Q.; Yang, D.; Huang, X. H.; Tu, J. P. Porous Co_3O_4 Nanotubes Derived from $Co_4(CO)_{12}$ Clusters on Carbon Nanotube Templates: A Highly Efficient Material For Li-Battery Applications. *Adv. Mater.* **2007**, *19*, 4505−4509.

(31) Fu, L.; Liu, Z.; Liu, Y.; Han, B.; Hu, P.; Cao, L.; Zhu, D. Beaded Cobalt Oxide Nanoparticles along Carbon Nanotubes: Towards More Highly Integrated Electronic Devices. *Adv. Mater.* **2005**, *17*, 217−221.

(32) Shan, Y.; Gao, L. Formation and Characterization of Multi-Walled Carbon Nanotubes/Co_3O_4 Nanocomposites for Supercapacitors. *Mater. Chem. Phys.* **2007**, *103*, 206−210.

(33) Suzuki, T.; Yan, X.; Kitahama, Y.; Sato, H.; Itoh, T.; Miura, T.; Ozaki, Y. Tip-Enhanced Raman Spectroscopy Study of Local Interactions at the Interface of Styrene−Butadiene Rubber/Multi-walled Carbon Nanotube Nanocomposites. *J. Phys. Chem. C* **2012**, *117*, 1436−1440.

(34) Kang, Y.; Taton, T. A. Micelle-Encapsulated Carbon Nanotubes: A Route to Nanotube Composites. *J. Am. Chem. Soc.* **2003**, *125*, 5650−5651.

(35) Gonzalez-Dominguez, J. M.; Tesa-Serrate, M. A.; Anson-Casaos, A.; Diez-Pascual, A. M.; Gomez-Fatou, M. A.; Martinez, M. T. Wrapping of SWCNTs in Polyethylenoxide-Based Amphiphilic Diblock Copolymers: An Approach to Purification, Debundling, and Integration into the Epoxy Matrix. *J. Phys. Chem. C* **2012**, *116*, 7399−7408.

(36) Gerstel, P.; Klumpp, S.; Hennrich, F.; Poschlad, A.; Meded, V.; Blasco, E.; Wenzel, W.; Kappes, M. M.; Barner-Kowollik, C. Highly Selective Dispersion of Single-Walled Carbon Nanotubes via Polymer Wrapping: A Combinatorial Study via Modular Conjugation. *ACS Macro Lett.* **2014**, *3*, 10−15.

(37) Dong, Y.; He, K.; Yin, L.; Zhang, A. A Facile Route to Controlled Synthesis of Co_3O_4 Nanoparticles and Their Environmental Catalytic Properties. *Nanotechnology* **2007**, *18*, 4356021−4356026.

(38) Grzelczak, M.; Zhang, J.; Pfrommer, J.; Hartmann, J.; Driess, M.; Antonietti, M.; Wang, X. Electro- and Photochemical Water Oxidation on Ligand-Free Co_3O_4 Nanoparticles with Tunable Sizes. *ACS Catal.* **2013**, *3*, 383−388.

(39) Britz, D. A.; Khlobystov, A. N. Noncovalent Interactions of Molecules with Single Walled Carbon Nanotubes. *Chem. Soc. Rev.* **2006**, *35*, 637−659.

(40) Karousis, N.; Tagmatarchis, N.; Tasis, D. Current Progress on the Chemical Modification of Carbon Nanotubes. *Chem. Rev.* **2010**, *110*, 5366−5397.

(41) Banerjee, S.; Hemraj-Benny, T.; Wong, S. S. Covalent Surface Chemistry of Single-Walled Carbon Nanotubes. *Adv. Mater.* **2005**, *17*, 17−29.

(42) Gao, C.; Jin, Y. Z.; Kong, H.; Whitby, R. L. D.; Acquah, S. F. A.; Chen, G. Y.; Qian, H. H.; Hartschuh, A.; Silva, S. R. P.; Henley, S.; Fearon, P.; Kroto, H. W.; Walton, D. R. M. Polyurea-Functionalized Multiwalled Carbon Nanotubes: Synthesis, Morphology, and Raman Spectroscopy. *J. Phys. Chem. B* **2005**, *109*, 11925−11932.

(43) Deng, S.; Zhang, Y.; Brozena, A. H.; Mayes, M. L.; Banerjee, P.; Chiou, W.-A.; Rubloff, G. W.; Schatz, G. C.; Wang, Y. Confined Propagation of Covalent Chemical Reactions on Single-Walled Carbon Nanotubes. *Nat. Commun.* **2011**, *2*, 3821−3826.

(44) Esswein, A. J.; McMurdo, M. J.; Ross, P. N.; Bell, A. T.; Tilley, T. D. Size-Dependent Activity of Co_3O_4 Nanoparticle Anodes for Alkaline Water Electrolysis. *J. Phys. Chem. C* **2009**, *113*, 15068−15072.

(45) Casas-Cabanas, M.; Binotto, G.; Larcher, D.; Lecup, A.; Giordani, V.; Tarascon, J. M. Defect Chemistry and Catalytic Activity of Nanosized Co_3O_4. *Chem. Mater.* **2009**, *21*, 1939−1947.

(46) Hu, L. H.; Peng, Q.; Li, Y. D. Selective Synthesis of Co_3O_4 Nanocrystal with Different Shape and Crystal Plane Effect on Catalytic Property for Methane Combustion. *J. Am. Chem. Soc.* **2008**, *130*, 16136−16137.

(47) Heck, R. M.; Farrauto, R. J. Automobile Exhaust Catalysts. *Appl. Catal., A* **2001**, *221*, 443−457.

(48) Chun, S.-J.; Lee, S.-Y.; Jeong, G.-Y.; Kim, J. H. Fabrication of Hydrophobic Self-Assembled Monolayers (SAM) on the Surface of Ultra-Strength Nanocellulose Films. *J. Ind. Eng. Chem.* **2012**, *18*, 1122−1127.

(49) Jia, C.-J.; Schwickardi, M.; Weidenthaler, C.; Schmidt, W.; Korhonen, S.; Weckhuysen, B. M.; Schüth, F. Co_3O_4−SiO_2 Nano-composite: A Very Active Catalyst for CO Oxidation with Unusual Catalytic Behavior. *J. Am. Chem. Soc.* **2011**, *133*, 11279−11288.